The Astronomical Journal, 147:86 (14pp), 2014 April doi:10.1088/0004-6256/147/4/86

FROM BINARIES TO MULTIPLES. I. DATA ON F AND G DWARFS WITHIN 67 pc OF THE SUN

Andrei Tokovinin
Cerro Tololo Inter-American Observatory, Casilla 603, La Serena, Chile; atokovinin@ctio.noao.edu
Received 2013 November 28; accepted 2014 January 24; published 2014 March 14

ABSTRACT

Data on the multiplicity of F- and G-type dwarf stars within 67 pc of the Sun are presented. This distance-limited sample based on the *Hipparcos* catalog contains 4847 primary stars (targets) with $0.5 < V - I_C < 0.8$ and is >90% complete. There are 2196 known stellar pairs; some of them belong to 361 hierarchical systems from triples to quintuples. Models of companion detection by radial velocity, astrometric acceleration, direct resolution, and common proper motion are developed. They serve to compute completeness for each target, using the information on its coverage collected here. About 80% of companions to the primary stars are detected, but the census of subsystems in the secondary components is only about 30%. Masses of binary components are estimated from their absolute magnitudes or by other methods; the periods of wide pairs are evaluated from their projected separations. A third of binaries with periods shorter than ∼100 yr are spectroscopic and/or astrometric pairs with yet unknown periods and mass ratios. These data are used in the accompanying Paper II to derive unbiased statistics of hierarchical multiple systems.

Key words: binaries: general – stars: solar-type – stars: statistics

Online-only material: color figure, machine-readable and VO tables

1. GOALS AND STRATEGY

Statistics of stellar multiple systems is important for several reasons, the major one being probably star formation. Why are some stars born with stellar companions and some not? What is the relation between multiplicity, debris disks, and planetary systems? Are stellar mergers in multiple systems frequent, and how do they affect the initial mass function? Compared to binaries, hierarchical multiples with three or more components contain additional information such as period ratios, mass ratios, and relative orbit orientation. Extracting and deciphering this information will help to understand star formation and, eventually, to predict statistics of stellar systems. Stellar hierarchies matter because they evolve differently from simple binaries, helping to form close binaries (Fabrycky & Tremaine 2007) and more exotic objects like blue stragglers (Peters & Fabrycky 2009). Hierarchical systems cause false positives in the search of exoplanets (Santerne et al. 2013).

The goal of this work is to establish unbiased statistics of hierarchical stellar systems (triples, quadruples, etc.). Previous studies focused mostly on binaries and considered multiples only in passing. While reaching completeness for binaries is difficult, it becomes even more problematic for hierarchies. As hierarchical systems are less frequent than binaries, their study requires larger samples. For example, the 25 pc volume surveyed by Raghavan et al. (2010) contains only 454 targets, 56 of which (12%) are triple or higher-order multiples—too few to grasp the statistics of hierarchies.

We extend the horizon of previous multiplicity studies to the distance of 67 pc, with 10× more objects. Solar-type dwarfs are chosen as primary targets, and a well-defined volume-limited sample is constructed from the *Hipparcos* catalog (Perryman & ESA 1997). Solar-type dwarfs are traditionally selected for multiplicity study because stars of lower mass are faint, while more massive stars are rare and distant. Although the knowledge of multiplicity in different mass regimes and environments is needed, nearby dwarfs are the first and easiest step toward this goal.

Our task is simplified by the existence of extensive data on nearby stars. Many targets are being monitored for exoplanets in radial velocity (RV), providing at the same time strong constraints on stellar companions. Collection of published data (data-mining) is the cornerstone of this study. It is complemented by small surveys designed to fill the lacking information. Instead of attempting to observe all ∼5000 stars with complementary techniques required to detect companions over the full range of periods and mass ratios, we explore specific areas of the parameter space. Particular attention is directed to binaries, trying to convert them into triples and to constrain the frequency of subsystems. Detection limits of various techniques are quantified and used to correct the remaining incompleteness.

Many stars in this sample host known exoplanets; more planets will be discovered in the future. Here we focus on *stellar* companions and mention exohosts only in the notes. Study of planets in stellar multiple systems is an interesting research topic (Roell et al. 2012), and it will be advanced by this data collection.

In the accompanying Paper II we present the statistical analysis of stellar hierarchies and place it in the context of prior work, while this first part (Paper I) contains the data. It begins by the definition of the sample in Section 2, followed by the review of data sources and methods in Section 3. Evaluation of detection completeness is covered in Section 4. Tables containing information on individual components and systems are presented in Section 5. The paper concludes by the overview of this data collection in Section 6.

2. THE FG-67 SAMPLE

Targets for this survey are selected from the *Hipparcos-2* catalog (van Leeuwen 2007, hereafter HIP2) by the following criteria.

1. Trigonometric parallax $p_{\rm HIP} > 15$ mas (within 67 pc of the Sun, distance modulus $<4.12^m$). Targets with parallax error >7.5 mas are excluded.

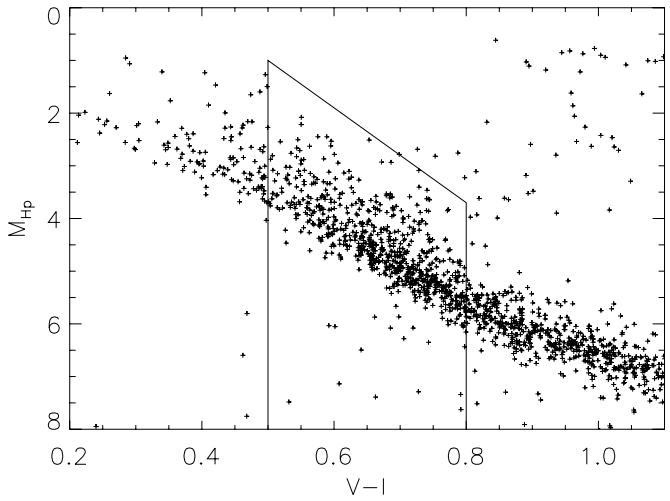

Figure 1. Color–magnitude diagram. The lines denote the selection criteria of the FG-67 sample. Only *Hipparcos* stars with $p_{\rm HIP} > 30$ mas are plotted.

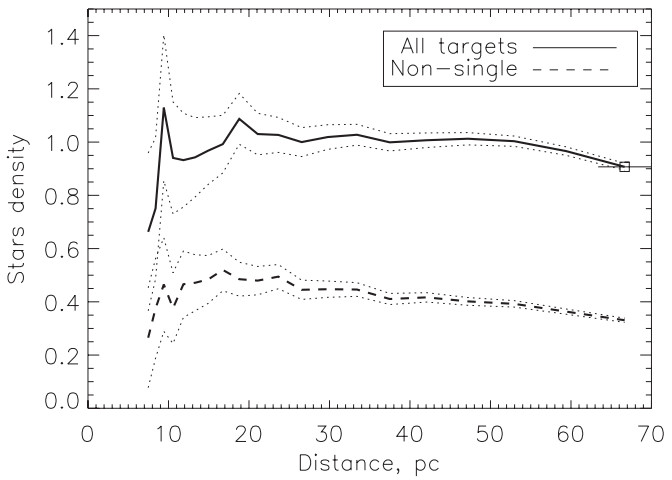

Figure 2. Density of FG-67 targets within given distance, normalized by 0.0043 star pc^{-3} (thick solid line). The thick dashed line shows the density of non-single targets. Dotted lines indicate the $\pm\sigma$ statistical errors; the square with a horizontal bar indicates a typical distance error.

2. Color $0.5 < V - I_C < 0.8$ (this corresponds approximately to spectral types from F5V to G6V, masses from 0.85 to 1.5 $M_\odot$).
3. Unevolved, satisfying the condition $M_{\rm Hp} > 9(V-I_C)-3.5$, where $M_{\rm Hp}$ is the absolute magnitude in the *Hipparcos* band calculated with $p_{\rm HIP}$. Subgiants are included in the sample.

Figure 1 shows the ($M_{\rm Hp}$, $V - I_C$) color–magnitude diagram (CMD) of *Hipparcos* stars. The upper cutoff in absolute magnitude is set at about 2^m above the main sequence to avoid discrimination against multiple stars. The Hyades cluster is included in the sample.

The criteria formulated above select 5040 stars from HIP2. However, components of wide binaries with two individual HIP entries must be counted only once (their secondaries are removed from the target list, even though they fulfill the sample criteria). We also removed targets that have wide companions more massive than 1.5 $M_\odot$. About 50 other targets (1%) are removed for various other reasons, e.g., stars located far below the main sequence (see Figure 1) and stars with erroneous $V-I_C$ colors in HIP2 (checked against photometry in other bands and/or spectral type). Cleaning reduces the original selection by 4%, leaving 4847 targets (primary components).

The selection criteria are blurred by observational errors in colors (the vertical lines in Figure 1 are not sharp) and distances. The actual errors of *Hipparcos* parallaxes sometimes exceed their formal errors, especially for binaries. We do not reject targets near the 15 mas cutoff if they appear to be farther away based on photometry. Some solar-mass stars within 67 pc are missed in the FG-67 sample because they were not included in the *Hipparcos* catalog, for example, the nearby multiple systems ζ Cnc and ξ UMa. The masses of primary components in the FG-67 sample are larger than in the 25 pc sample of Raghavan et al.; the lower cutoff in mass is dictated here by the completeness of the *Hipparcos* catalog. For this reason, the size of the FG-67 sample is less than the size of the 25 pc sample scaled as a cube of the distance limit.

Completeness of the FG-67 sample is illustrated in Figure 2. The number of targets within distance d is proportional to d^3, so their spatial density is nearly constant, dropping only by 10% at 67 pc. A drop of 8% is expected if the vertical scale of the Galactic disk is 300 pc, so the completeness of the present sample is above 90%. The density of 1769 non-single targets declines with distance slightly faster, indicating progressively increasing incompleteness of the binary census. The observed multiplicity fraction is therefore $f_M = 1769/4847 = 0.36$, to be compared to the true $f_M = 0.46$ derived by Raghavan et al. (2010) and confirmed in Paper II. The overall completeness of companion detection is reasonably high, about 80%.

3. DATA SOURCES AND METHODS

3.1. Data Structure

All data on a given system are linked by the *Hipparcos* number of its primary component, HIP0. Four tables, presented in detail in Section 5, contain information on the individual components (COMP), binary pairings (SYS), detection limits (DET), and notes (NOTES), as illustrated in Figure 3. Custom software written in IDL helps to maintain this database: browse and edit the data, evaluate system parameters and companion detection probability, query some catalogs. Components can be placed on the (V, $V - K$) or (J, $J - K$) CMDs to check the consistency of their parallax. Colors in various passbands are checked for consistency with colors of main-sequence dwarfs.

Each binary system has two important attributes. The first, component designation, describes the hierarchy by a comma-separated list of three components (primary, secondary, parent). For example, the visual binary HIP 518 has components A,B,* (asterisk in place of the parent denotes the *root* of the hierarchy, i.e., the outermost pair). The spectroscopic subsystem in the secondary component is Ba,Bb,B. This designation is explained in Tokovinin et al. (2006) and is now used in the Multiple Star Catalog (Tokovinin 1997).

The second attribute is the *type* of the system, meaning discovery techniques such as spectroscopic binaries (type "s"), visual binaries (type "v"), etc., as detailed further in this section. The type determines the sense of system parameters such as separation and period; they are either derived from the orbital solutions or estimated (Section 3.9). A system can have several types.

3.2. Bibliographic References and Their Codes

Periods of binary systems span a huge range, from a fraction of a day to megayears. To reach completeness, combination of

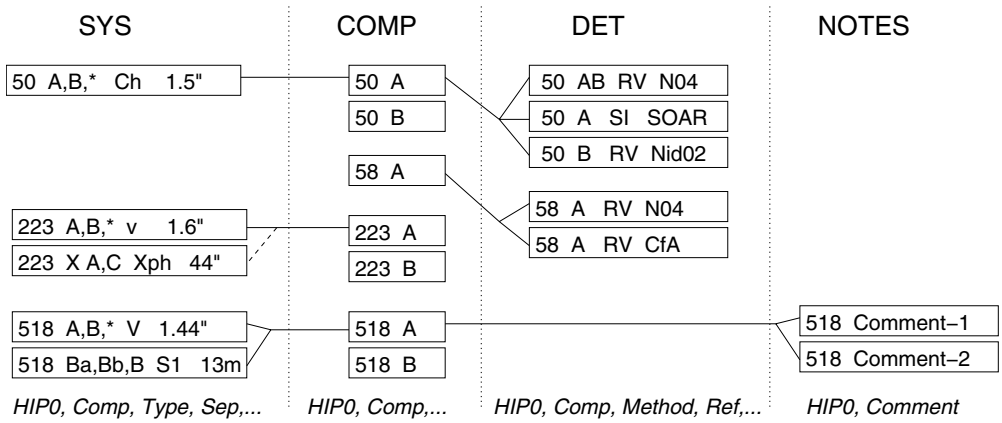

Figure 3. Data structure. The four tables SYS, COMP, DET, and NOTES are related by HIP0, the *Hipparcos* number of the primary component. The examples show binary systems 50 and 223 (the latter with an optical companion C), a single star 58, and a triple system 518. Each target can have an arbitrary number of records in the SYS, DET, and NOTES tables.

various observing techniques and data sources is mandatory. This work takes full advantage of extensive data on nearby stars collected by generations of astronomers. To a large extent it relies on compilations and catalogs. Instead of giving proper credit to the original authors (which would require several thousand references), we cite the catalogs whenever possible. References on individual objects can be obtained from SIMBAD. This data collection is reasonably complete, but not free from omissions. We checked bibliographic references only for a subset of targets. Most information was collected by systematic scanning of major astronomical journals (up to 2013 November 1) and complemented by some unpublished work mentioned further in this section.

Table 1 lists major sources used in this survey, in alphabetic order of the reference codes adopted here. The last column contains a short comment on the nature of data and, where appropriate, gives the number of targets covered. In addition, stellar parameters such as effective temperature and abundance for many FG-67 targets can be found in the PASTEL catalog (Soubiran el al. 2010). RVs and kinematics are collected in the XHIP (Anderson & Francis 2012). These compilations complement the multiplicity data collected here.

3.3. Standard Relations

Stars on the main sequence show tight relation of their mass with effective temperature (hence spectral type and color) and absolute magnitude. As distances to our targets are known, we estimate mass from absolute magnitude using standard relations. Luminosity is a strong function of mass, reducing the influence of errors in distance or photometry (e.g., additional light from unresolved binary companions) on the estimated masses.

Relations between mass and absolute magnitude for the main-sequence stars are established both empirically (Henri & McCarty 1993; Delfosse et al. 2000; Lang 1992) and through stellar models (Baraffe et al. 1998; Girardi et al. 2000). For dwarfs of $M < 1\,M_\odot$, the agreement between these sources is generally good, on the order of $0\overset{\mathrm{m}}{.}2$ in absolute magnitude. We merged various standard relations in a table of absolute magnitudes versus mass for a grid of stellar masses from 0.075 $M_\odot$ to 2 $M_\odot$. For each mass, the curve $M_{\rm abs}(k = 1/\lambda)$ is almost linear, so its cubic approximation is good to $\sim 0\overset{\mathrm{m}}{.}1$. Here λ is the central wavelength of photometric bands, assumed to be [550, 770, 1250, 2200] nm for the V, I_C, J, K_s bands, respectively. Polynomial approximations allow us to interpolate

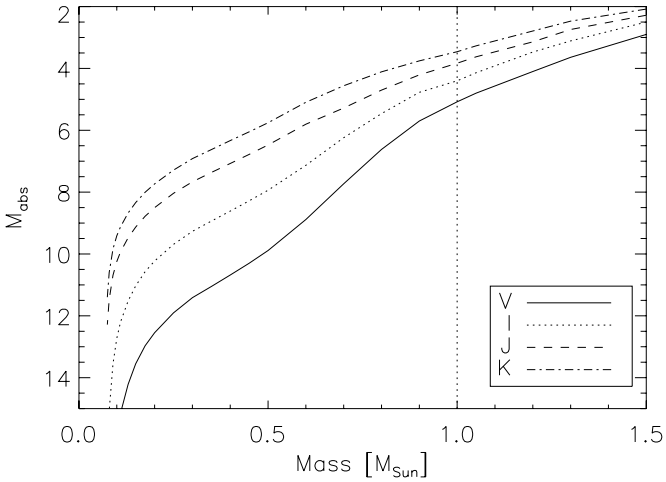

Figure 4. Standard relations for main-sequence stars: absolute magnitude in several photometric bands vs. mass.

standard relations $M_{\rm abs}(\lambda)$ to other wavelengths. They are plotted in Figure 4. For a star of 1 $M_\odot$, the polynomials give absolute magnitude of [5.08,4.40,3.83,3.46] in the V, I_C, J, K_s bands, respectively.

The estimated masses of binary components are based on their absolute V magnitudes (code "v" for the mass) or, in a few occasions, on the infrared magnitudes (code "k"). The values are interpolated linearly in the $M_{\rm abs}$, M table. We compared masses of single stars with masses estimated by Casagrande et al. (2013) from evolutionary tracks and found a good correspondence. However, the masses estimated here are on average 9% larger. Subgiants are brighter and more massive than main-sequence stars; they extend the upper mass limit of this sample to $\sim$1.7 $M_\odot$. There are 63 targets with $M > 1.5\,M_\odot$ and 10 targets with $M < 0.85\,M_\odot$; the remaining 98.5% have masses within these limits. The median mass of the primary targets is 1.14 $M_\odot$.

The following subsections review data on binaries by the type of their discovery technique, in order of increasing period.

3.4. Spectroscopic Binaries (S1, S2, s)

Most spectroscopic binaries (SBs) with known orbits are retrieved from the online SB9 catalog (Pourbaix et al. 2004), complemented by recent publications where necessary. Single- and double-lined binaries have types "S1" and "S2,"

Table 1
Bibliographic References and Their Codes

Code	Reference	Comment, Number of Targets
2MASS	Cutri et al. (2003)	J, H, K, companions 5″ to 30″
Abt2006	Abt & Willmarth (2006)	RV (143)
ANDICAM	Tokovinin (2011)	2MASS companions (66)
CfA	D. W. Latham (2012, private communication)	RV (1839)
Chauvin06	Chauvin et al. (2006)	AO, exohosts (17)
Chauvin10	Chauvin et al. (2006)	AO, young stars (9)
Egg2007	Eggenberger et al. (2007)	AO, exohosts (86)
Ginski2012	Ginski et al. (2012)	Lucky imaging, exohosts (24)
Gorynya2013	N. A. Gorynya (2014, in preparation)	SB orbits (7)
Griffin2012	Griffin (2012)	SBs in Hyades
Halb2012	Halbwachs et al. (2012)	RV of CPM pairs (10)
Hartkopf2013	Hartkopf et al. (2013)	CPM pairs (18)
HIP1	Perryman & ESA (1997)	Resolved binaries
HIP2	van Leeuwen (2007)	Position, parallax, PM, V, I_C
Horch2011	Horch et al. (2011)	Speckle interferometry (9)
INT4	Hartkopf et al. (2001)	Speckle interferometry and AO
Jenkins2010	Jenkins et al. (2010)	AO, exohosts (4)
Jodar2013	Jódar et al. (2013)	Low-mass companions (6)
Jones2002	Jones et al. (2002)	Precise RV (156)
LAF07	Lafrenière et al. (2007)	AO (20)
Lagrange09	Lagrange et al. (2009)	RV (41)
Latham2002	Latham et al. (2002)	RV (236)
LEPINE	Tokovinin & Lépine (2012)	CPM ($\rho > 30''$)
MH09	Metchev & Hillenbrand (2009)	AO (122)
MK05	Makarov & Kaplan (2005)	Acceleration binaries
MSC	Tokovinin (1997)	Multiple systems
N04	Nordström et al. (2004)	RV (4080)
NICI	Tokovinin et al. (2012, 2013)	AO (107)
Nid02	Nidever et al. (2002)	Precise RV (438)
NOMAD	Zacharias et al. (2004)	Photometry and PM of secondaries
R10	Raghavan et al. (2010)	Stars within 25 pc
Rameau2013	Rameau et al. (2013)	AO (12)
RoboAO	Riddle et al. (2014, in preparation)	AO (704)
SB9	Pourbaix et al. (2004)	Spectroscopic binaries
SEEDS	Janson et al. (2013)	AO (15)
SO2011	Shaya & Olling (2011)	Very wide pairs
SOAR	Tokovinin et al. (2010a), other	Speckle interferometry (604)
TS02	Tokovinin & Smekhov (2002)	RV of visual binaries (104)
Tok2006	Tokovinin et al. (2006)	AO (31)
Tok2010	Tokovinin et al. (2010a)	AO (62)
Tremko2010	Tremko et al. (2010)	RV (5)
VB6	Hartkopf & Mason (2013)	Visual orbits
WDS	Mason et al. (2001)	Visual & CPM companions
WSI	B. D. Mason (2009, private communication)	Speckle interferometry (1723)

respectively. The masses of the secondary components are derived either from the known mass ratio in the case of S2 (mass code "q") or as a minimum mass for orbital inclination of 90° inferred from the mass function and the mass of the primary component (mass code "m").

A large fraction of our sample (84%) was surveyed in RV by Nordström et al. (2004). For 261 stars, variable RV was detected, but their orbits are not known. Such cases are coded by "s" in the system type. When double lines were seen in several spectra (type s2), the mass ratios were derived, while the orbital period still remains unknown. Preliminary orbital solutions for many binaries were obtained at Center for Astrophysics (CfA) by D. W. Latham (2012, private communication), extending the survey by Latham et al. (2002). In some cases, only the orbital period is known to the author, leaving the minimum secondary mass undetermined. For double-lined binaries with known period and unknown RV amplitudes, the mass ratio of 0.8 is assumed (this is the median value for all S2), and the secondary mass code in this case is "e" (estimated). Orbits of several short-period binaries discovered by Nordström et al. (2004) and not covered by CfA were recently determined by N. A. Gorynya (2014, in preparation).

The large volume of precise RV data accumulated in search of exoplanets remains, for the most part, unpublished and inaccessible, with a few exceptions (Nidever et al. 2002; Jones et al. 2002). Tokovinin & Smekhov (2002) monitored RVs of visual binaries to characterize the frequency of spectroscopic subsystems, and Halbwachs et al. (2012) studied RVs of wide common proper motion (CPM) pairs. The work of Griffin (2012) demonstrates the power of long-term RV monitoring by detecting all SBs in the Hyades.

Some close binaries are eclipsing. They have type "E" (26 total). Most of them also have known spectroscopic orbits. Considering the RV coverage, we did not search for eclipsing

binaries systematically and do not account for detection of eclipsing binaries in this study.

3.5. Astrometric Binaries (a, A)

Binary stars are detectable from their accelerated motion (Makarov & Kaplan 2005; Frankowski et al. 2007). In some cases, acceleration was measured by the *Hipparcos* mission over its 3.2 yr duration; these stars are known as $\dot{\mu}$ binaries or G-type solutions. In addition, accelerated motion in the so-called $\Delta\mu$ binaries is revealed by a significant difference between the short-term *Hipparcos* proper motion (PM) and the long-term PM from the *Tycho-2* catalog exploiting a time base of almost a century. Acceleration binaries of both kinds are coded by type "a." For a fraction of them, astrometric orbital solutions were derived in the original *Hiparcos* catalog or later (e.g., Goldin & Makarov 2006). In those cases (type "A"), the orbital periods are known. Combining periods with estimated masses of primary components and the distance, we compute the apparent semi-major axis a from the third Kepler law. The ratio of the astrometric axis to a allows us to estimate the mass ratio of A-type binaries (mass code "q").

So far, little is known about unresolved acceleration binaries (some of those are also s-type, i.e., have variable RV but no SB orbits). Yet they cover an important range of orbital periods from a few to a hundred years where alternative detection techniques are not very efficient, especially for low-mass companions. A subset of these stars were targeted by a dedicated adaptive optics (AO) survey at Gemini-S (Tokovinin et al. 2012, 2013). About a third were resolved (turned into type "v"), allowing estimates of the companion's mass and orbital period. The remaining acceleration binaries have companions too faint and/or too close to be resolved. Some of those unresolved companions could be white dwarfs (WDs).

The Gemini survey revealed new things about acceleration binaries. It was established that some acceleration solutions are spurious, resulting from the ill-conditioned least-squares problem. The new *Hipparcos* reduction, HIP2, eliminated most of those solutions, but missed many real acceleration binaries, thus being of little help. Some stars with $\dot{\mu}$ accelerations actually are relatively wide binaries resolved with AO (Tokovinin et al. 2013)—too wide to explain the acceleration. This group is a mixture of spurious accelerations where astrometric "noise" from faint companions was amplified in ill-conditioned solutions, and triple stars where the accelerations are produced in the inner subsystems.

Our simulations demonstrated that most $\dot{\mu}$ binaries are also detectable by the $\Delta\mu$ method. Therefore, in this work we consider only $\Delta\mu$ astrometric binaries and do not accept $\dot{\mu}$ binaries as real unless they are confirmed by other methods or have known astrometric orbits.

3.6. Close Resolved Binaries (v, V)

In the resolved binaries, the companion is detected by its light, unlike the RV and acceleration methods, where only its gravity matters.

The *Hipparcos* experiment provided companion solutions (i.e., resolved visual binaries) with a more or less uniform detection depth for all targets, as needed for this statistical work. In addition, close pairs resolved by speckle interferometry and AO are collected in the INT4 catalog (Hartkopf et al. 2001), and all known visual and occultation binaries are cataloged by the Washington Double Stars (WDS, Mason et al. 2001). These inhomogeneous data come from various sources.

Most visual binaries with separation under $3''$ are denoted as type "v" and are assumed to be physical systems, considering the small probability of finding a random (and usually bright) star at such small separations. Whenever visual orbits are available in the VB6 catalog (Hartkopf & Mason 2013), the type becomes "V" and we list the true orbital period and semi-major axis instead of separation. Otherwise, the orbital period P^* is estimated from the separation (see Section 3.9).

3.7. Wide Companions (C)

Many wide companions listed in the WDS are chance projections (optical), denoted as type "X." This can be revealed by their fast relative motion incompatible with a Keplerian orbit, or by the companion's magnitude and color that do not match the values expected for a main-sequence dwarf at the same distance as the primary, or by the difference in RV. When the apparent motion in a wide pair is caused by the PM of its primary component—*reflex PM*—its optical nature is obvious. On the other hand, when the wide companion is real (physical), it is denoted as type "C" with following small-letter qualifiers h, m, p, r that show which criteria of physical relation are fulfilled: constant relative position, common PM, matching photometric distance, or matching RV (see details in Tokovinin 1997). Optical companions may also have these qualifies to show which criterion was used for their rejection. Optical systems from the WDS and other doubtful binaries are included in the SYS table for completeness (e.g., HIP 223 A,C in Figure 3), but are ignored in the statistical analysis.

Binary companions with separations from $5''$ to $30''$ can be found in the Two Micron All Sky Survey (2MASS) Point Source Catalog, with well-defined detection limits. This is a valuable complement to the heterogeneous data of WDS, especially in the low-mass regime (Tokovinin 2011). The photometry in 2MASS discriminates against unrelated (optical) stars, but only out to moderate separations and in not too crowded fields. At small separations $\rho \lesssim 5''$, the 2MASS photometry of faint components is usually distorted by bright primaries, so case-by-case checks are necessary (we ignore close 2MASS pairs that do not have additional evidence of their veracity). On the other hand, contamination by the field stars becomes important at $\rho \gtrsim 10''$. This is why second-epoch imaging was needed to confirm candidate companions found in 2MASS. The work, started in Tokovinin (2011), was extended to $\rho < 30''$ (unpublished results of this extension are mentioned in the notes as ANDICAM2), but it does not cover the northern sky. Physical nature of some northern candidates found in 2MASS could be confirmed by archival optical images or PMs. Overall, 43 binaries from 2MASS are added here to the 47 new pairs confirmed in (Tokovinin 2011).

Components of some wide binaries have different parallaxes in *Hipparcos*, for example, 20 ± 5 mas and 8 ± 3 mas for HIP 76888 and 76891, respectively. Yet this is a physical binary STF 1966 with $23''$ separation observed for 173 yr. The photometric parallax of both components is slightly less than 15 mas. There was a problem in the *Hipparcos* data reduction for binaries with separations around $20''$ or binaries containing subsystems, like HIP 43947 (Tokovinin et al. 2010a). In those instances we adopt the same parallax for both components.

At separations $\rho > 30''$, both photometry and PM are needed to distinguish true (physical) companions from other stars. Uniform screening of stars within 67 pc for wide companions down to $V = 19$ became possible with the SUPERBLINK survey (Tokovinin & Lépine 2012), except 39% of targets with

small PM. In that work, the probability of each companion being physical was estimated. Here we accept all CPM companions with probability of >50% and add some lower-probability candidates with a high PM or other indications that they are real pairs. Subjective decisions on the status of some wide companions were thus made.

In addition to the SUPERBLINK survey, CPM pairs were retrieved from the WDS (including the recent addition by Hartkopf et al. 2013) and by matching the *Hipparcos* catalog entries in PM and parallax. The latter method was also used by Shaya & Olling (2011) to identify very wide co-moving pairs or groups of stars. These pairs are members of kinematic groups rather than bound binaries; hence, we do not include them in the SYS table, but mention them in the notes. There is no clear distinction between true (bound) wide binaries and members of moving groups (Caballero 2010). Members of the Hyades cluster have common PM and distance, but are not binaries.

The probability of finding false CPM companions is larger for targets with small PM and/or in crowded fields. If a substantial fraction of CPM companions were optical, we expect such pairs to have smaller PM and larger crowding N^*. Comparison of the median PM and crowding for 335 binaries with $\rho > 30''$ (133 mas yr^{-1} and 16, respectively) with the medians for the complete sample (125 mas yr^{-1} and 22) shows the opposite trend. Statistically, the sample does not contain false wide binaries and might actually miss some real CPM binaries.

3.8. Dedicated Surveys

Nearby stars within 25 pc were thoroughly surveyed by Raghavan et al. (2010). We include information from that work and use it as a check of completeness. Despite substantial observational effort, parameters of a few nearby binaries were still undetermined and had to be "guessed." There are 243 targets (out of 454) in common with this work; the rest have masses smaller than the FG-67 limit. Interestingly, Raghavan et al. list three hierarchical multiples with five to six components (HD 68257, 146361, 186858). The first is missed here because it has no HIP number; the last is only a quadruple (the RV variability of the component F = HIP 97222 is questioned). Despite the 10× larger size of the present sample, it contains only five known quintuples (of which just one, HD 146361 = HIP 79607, is within 25 pc) and no sextuple systems.

Only a small fraction of nearby dwarfs were targeted by AO in search of companions to exoplanet hosts (Eggenberger et al. 2007), to spectroscopic binaries (Tokovinin et al. 2006), or to young stars (Metchev & Hillenbrand 2009; Chauvin et al. 2010). In the context of this project, we surveyed with AO wide binaries (Tokovinin et al. 2010a) and astrometric binaries (Tokovinin et al. 2012, 2013).

Speckle interferometry and lucky imaging in the visible do not go as deep as AO, but cover a larger number of stars owing to their better efficiency. Many FG-67 targets were observed with speckle interferometry at the SOAR telescope (Tokovinin et al. 2010b, and following papers), discovering new close subsystems in visual binaries, resolving some acceleration binaries, and following the orbital motion of "fast" close pairs. Some unpublished speckle data on G-dwarfs were provided by B. Mason (2009, private communication); they are referenced as WSI (Washington Speckle Interferometry) in the DET table.

Almost 600 stars from the FG-67 were recently targeted by the RoboAO system at the 1.5 m Palomar telescope (Riddle et al. 2014, in preparation). This work focused on resolving faint secondary components to constrain their poorly known multiplicity. In addition, many close binaries were observed to look for more distant and faint tertiary companions.

3.9. Estimation of Binary Parameters

As mentioned above, the exact meaning of separation and period in the SYS table depends on the system type. These parameters, as well as masses, are estimated automatically by a recursive algorithm that takes care of subsystems. For each target (HIP0 number), it selects the data on all its systems and finds the outermost binary, the root. Each component of this binary is checked for the presence of subsystems, using the parent name in the system designation. The subsystem, when present, is evaluated first, and the mass sum is assigned to its parent with a code "s" (sum).

For systems of types S1, S2, A, and V, the true orbital periods are known. In addition, the V-type systems have known semi-major axis; only the masses of both components need to be evaluated. Cases where the mass sum inferred from the visual orbit and parallax differs significantly from the estimated sum of the component's masses are commented, usually indicating poor quality of the visual orbit.

For resolved systems with unknown periods (types v, C), a probable orbital period P^* is found by the third Kepler law by assuming that the angular separation ρ equals orbital semi-major axis a,

$$P^* = \left[\rho^3\, p_{\rm HIP}^{-3}(M_1 + M_2)\right]^{1/2}, \quad (1)$$

where $p_{\rm HIP}$ is the parallax of the main target, M_1 and M_2 are masses of components in units of solar mass, and P^* is the estimated period in years. Simulations of binary stars with random orbital phases and eccentricities show that the median ratio ρ/a is indeed close to 1, depending slightly on the eccentricity distribution. For a cosine e-distribution with $\langle e\rangle = 0.5$, the 10%, 50%, and 90% quantiles of the ρ/a ratio are 0.38, 0.90, and 1.42, respectively. If the eccentricity distribution is linear, $f(e) = 2e$, these quantiles are 0.37, 0.98, and 1.59. In any case, $\rho/a < 2$, so the ratio of estimated and true periods P^*/P does not exceed $2^{3/2} = 3.17$. By assuming $a = \rho$, we estimate orbital periods to within a factor of 3, typically.

For the unresolved binaries with known period (types S1, S2, A), we use the same formula to estimate the orbital semi-major axis, which is listed in place of the separation. The separation of resolved pairs is not replaced by those estimates, however. The value of separation for resolved binaries with detectable motion is ambiguous; usually it corresponds to the latest measured separation listed in the WDS or INT4.

The program that computes binary periods or separations also assigns masses to the components. When the visual magnitudes are listed, the masses are evaluated from the absolute V-magnitudes and receive the code "v." When the magnitude difference of a binary is measured at some wavelength and the total combined V magnitude is known, we solve for component masses that match those two numbers and the distance, using standard relations. For systems of types S1 and S2, the secondary mass has codes "m" (minimum) and "q," respectively. The mass code "q" is also assigned to the secondary components of systems with astrometric orbits (type A). Finally, the code "r" means that the component's masses are taken from the literature; these masses are not overridden by any of the above estimates.

A summary of system types, corresponding meaning of the separation and period in the SYS table, and codes of secondary masses is provided in Table 2. Spectroscopic and acceleration

Table 2
System Types and Parameters

Type	Sep.	Per.	M_2 Code
Spectroscopic (S1, S2)	a	P	m, q
Spectroscopic (s)	0	0	...
Astrometric (A)	a	P	q
Acceleration (a)	0	0	...
Visual (V)	a	P	v, k
Visual (v)	ρ	P^*	v, k
Wide (C)	ρ	P^*	v, k
Optical (X)	ρ	0	...

binaries with unknown orbits are the worst case: we do not know their periods, separations, and mass of the secondary components. All these fields have the default zero values in the SYS table.

3.10. False and Dubious Binaries

Some stars declared to be binaries are in fact single. Spurious discoveries are produced by all techniques discussed above. For example, one slightly deviant RV measure can cause a formal detection of RV variability of a single star. Some accelerations in *Hipparcos* are spurious. Visual observers and speckle interferometry alike produced a number of false resolutions of single stars or subsystems, sometimes with several "confirming" measurements. Finally, the physical nature of some wide CPM pairs is uncertain, especially when the PM is small and the field is crowded. On the other hand, apparent motion of a rejected wide binary, deduced from the first and last observations listed in the WDS, can appear too fast simply because the measurements are inaccurate.

In this work, decisions on accepting or rejecting binary pairs are taken on the basis of available data, which are not always conclusive. Such cases are marked by the question mark in the system type. There are 346 question marks, about 10% of all systems. Of those, 115 are type "a" (rejected accelerations), 75 type "s" (uncertain RV variability), 99 type "C" (uncertain CPM pairs), and 35 type "v" (spurious resolutions). Some subjectivity is therefore unavoidable in this work. The actual proportion of wrongly accepted or rejected binary pairs should be much less than 10%, but it is difficult to evaluate.

3.11. White Dwarf Companions

Some FG-type dwarfs were originally paired to more massive stars that evolved and became WDs. Those "Sirius-like" binaries where a WD is paired to a main-sequence star (Holberg et al. 2013) are difficult to detect. Holberg et al. estimate the density of such pairs in the 20 pc volume as 3.3×10^{-4} pc^{-3} and their fraction among main-sequence stars as less than 1.2%. His table contains 15 WD binaries with components of spectral types F5V to G6V located within 67 pc (three of those are not in this sample because they are not present in *Hipparcos*). Three of those binaries are within 20 pc, giving a rather uncertain estimate of WD fraction in the FG-67 sample as 2%. This fraction rises to 4% if we take the above density of Sirius-like binaries, suppose that half are paired to the F- or G-stars, and compare with the spatial density of our targets, 4.3×10^{-3} pc^{-3} (Figure 2). Actually, 22 binaries are known or suspected to contain WD companions (HIP numbers: 11028, 18824, 20284, 27878, 29788, 32329, 37853, 54530, 60081, 64150, 77358, 80182, 80337, 81478, 81726, 83431, 95293, 99956, 103735, 104101, 113231, 118010), 14 of them with separations above 30″. The majority of Sirius-like binaries in the FG-67 sample remain undetected, but some may hide among the acceleration binaries.

4. DETECTION LIMITS

Knowledge of the probability of the companion's detection as a function of its orbital period P and mass ratio $q = M_2/M_1$ is necessary for deriving unbiased multiplicity statistics. Corrections for missed companions are larger for triples and quadruples than for binaries. If we detect companions with a probability of 0.8, the chance of discovering a triple system (two companions) is $0.8^2 = 0.64$. It can be even less because detection of subsystems in the *secondary* components of known binaries meets with additional difficulty. Raghavan et al. (2010) note that improved completeness of their survey did not change the binary fraction derived in earlier works (Duquennoy & Mayor 1991), but doubled the number of known hierarchies within 25 pc.

In this section, we present algorithms used to translate the observational coverage of each target or component (as listed in the DET table) to the detection probability in the (P, q) parameter space. The algorithm is rather straightforward in the case of direct resolution (AO imaging and speckle interferometry). We apply the default resolution limits of *Hipparcos* and 2MASS to all main targets and to some secondary components. In addition, the *Hipparcos* acceleration $\Delta\mu$ detects binaries with periods from a few to 100 years with a probability that is determined by simulations in Section 4.3. At shorter periods, the main discovery technique is spectroscopy, where the detection probability is also found by simulation and related to the number of observations, their precision, and time coverage (Section 4.2).

Resolution of a binary constrains, to some extent, subsystems in its secondary component. Similarly, RV data on an unresolved visual binary tell something about potential subsystems in its primary and secondary components. Detection of subsystems in the secondary components is also covered in this section. Binarity of secondary components was frequently neglected in previous works on multiplicity statistics.

The information on detection limits and their modeling are necessarily approximate. Here we tend to adopt optimistic (deeper) detection limits, so that the completeness correction becomes smaller and the estimated multiplicity becomes less. In other words, conservative estimate of multiplicity requires generous allocation of detection limits.

4.1. Resolved Binaries

Maximum magnitude difference of binaries resolved by *Hipparcos* (companion solutions) $\Delta\mathrm{Hp}(\rho)$ shows a well-defined limit depending on the angular separation ρ ($\Delta\mathrm{Hp} < 2.2$ at $\rho = 0\farcs14$ and $\Delta\mathrm{Hp} < 4$ at $\rho > 0\farcs4$). Similar limits exist for other imaging techniques like AO and speckle interferometry (see Table 3). They are translated to the detection limits in the (P, q) space in the following way. Each period P is converted to separation ρ using Equation (1). The absolute magnitude of the primary component at wavelength λ is computed from its mass M_1 using the standard main-sequence relation (Section 3.3). We add the maximum magnitude difference of detectable companions $\Delta m(\rho, \lambda)$, convert back into mass $M_{2,\min}$ with the same standard relation, and obtain $q_{\min} = M_{2,\min}/M_1$.

The detection limits of imaging techniques are represented here by four values of separation ρ_i, corresponding Δm_i, and the imaging wavelength λ. The ρ_1 and ρ_4 define the minimum and maximum range of surveyed separations, respectively,

Table 3
Representative Detection Limits for Resolved Binaries

Method	N	λ	ρ_1	ρ_2	ρ_3	ρ_4	Δm_1	Δm_2	Δm_3	Δm_4	Ref.
(1)	(2)	(3)	(4)	(5)	(6)	(7)	(8)	(9)	(10)	(11)	(12)
HIP1	all	550	0.09	0.14	0.4	10.0	0.0	2.2	4.0	4.3	Perryman & ESA (1997)
WDS	all	550	0.15	1.0	10.0	30.0	2.5	5.0	8.0	9.4	$5+3\log_{10}\rho''$
Speckle	604	540	0.03	0.15	1.00	1.50	0.50	4.33	5.63	5.63	Tokovinin et al. (2010a)
AO	122	2200	0.09	1.00	2.00	5.00	1.00	6.32	8.60	9.90	Metchev & Hillenbrand (2009)
AO	107	2272	0.054	0.15	0.90	9.00	0.0	5.42	7.48	7.48	Tokovinin et al. (2012, 2013)
2MASS	all	2200	3.0	9.0	20.0	30.0	0.0	7.5	10	11	Tokovinin (2011)

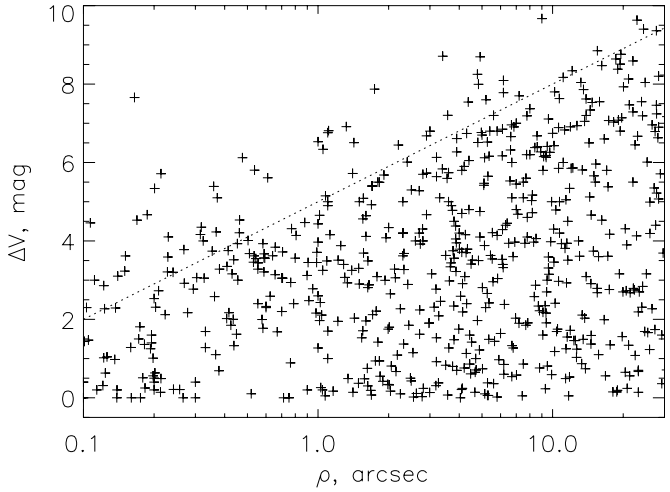

Figure 5. Magnitude difference vs. angular separation ρ for resolved binaries (types v and C) in the FG-67 sample. The dotted line is $\Delta V = 5+3\log_{10}(\rho)$.

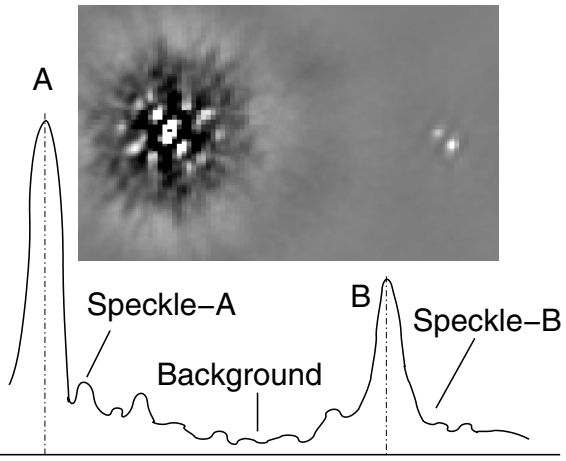

Figure 6. Detection of subsystems in the secondary components of resolved binaries. The image shows detection of the subsystem Ba,Bb (0.″12, $\Delta m = 0.9$) in the binary HIP 44874 AB (1.″79, $\Delta m = 4.8$) observed with speckle interferometry at SOAR in 2013. The curve illustrates noise in the image of a binary, dominated by the residual speckle structure near each component and by the background fluctuations away from them.

and $\Delta m(\rho)$ at intermediate separations is linearly interpolated between the four nodes, describing this curve by three linear segments. Obviously, this is a crude approximation, as well as the assumption that the probability of companion detection drops sharply from 1 to 0 at $q < q_{\min}$. Representative limits are given in Table 3. It lists the number N of targets from the FG-67 sample covered by each work, λ, ρ_i, median Δm_i, and the reference. We presume that all primary targets were examined by visual observers and adopt a somewhat optimistic limit

$$\Delta V < 5+3\log_{10}(\rho/1'') \quad (2)$$

which delineates the upper envelope of the companion distribution in the $(\rho, \Delta V)$ plane (dotted line in Figure 5).

Secondary components targeted *individually* by AO or speckle interferometry are treated in the same way as the primary targets. In addition, observations of a resolved binary AB place constraints on the existence of resolved companions (subsystems) around its secondary B. In hierarchical multiples, such subsystems can have separations $\rho < \rho_{AB}/2$ (otherwise, the subsystem cannot be attributed to B). The known detection limit $\Delta m_A(\rho, \lambda)$ on companions around A is translated into the limit on companions around B by assuming that both limits correspond to $5\sigma_I$, where the rms intensity fluctuation $\sigma_I(\rho)$ is the quadratic sum of the residual speckle noise (which dominates at small separations) and the background noise (Figure 6). In the vicinity of the secondary, the background noise and the scaled speckle noise define σ_I. This logic leads to the following formula (we omit here its derivation):

$$\Delta m_B(\rho) = -2.5\log_{10}[5\sigma_I(\rho)/I_B] \approx -1.25\log[10^{0.8[\Delta m_{\rm AB}-\Delta m_A(\rho_{\rm AB})]}+10^{-0.8\Delta m_A(\rho)}], \quad (3)$$

where $\Delta m_A(\rho)$ is the detection limit for the primary component A, $\rho_{\rm AB}$ is the separation of the AB binary, and $\Delta m_{\rm AB}$ is its magnitude difference. We compute the detection limits for subsystems around secondary components of resolved binaries using this formula.

Many wide binaries do not have any constraints on the binarity of their secondary components. Does this mean that the secondary component itself can be, say, a 5″ pair? Indeed, new close subsystems were discovered by the targeted survey of secondary components with Robo-AO (Riddle et al. 2014, in preparation). However, an obvious pair would be noted in the optical or infrared images even without dedicated observations. We presume (optimistically) that the detection limits of 2MASS apply to the secondary components with $\rho > 6''$, down to $K_s = 16$. This assumption constrains relatively wide secondary subsystems, which are not frequent anyway.

This reasoning could be extended to all binaries in the WDS. Indeed, some of them contain known subsystems in their secondaries. However, speckle interferometry at SOAR revealed many more such subsystems, previously missed by "visual" observers, like the one in Figure 6 (see also Tokovinin et al. 2010a). They were missed because instruments used normally to observe a 1″ binary have matched angular resolution and do not allow discovery of inner pairs with separations much smaller than 1″. Therefore, we do not apply the generic WDS limit (2) to the secondary components, except the eight historically resolved secondaries that do not have AO and speckle coverage.

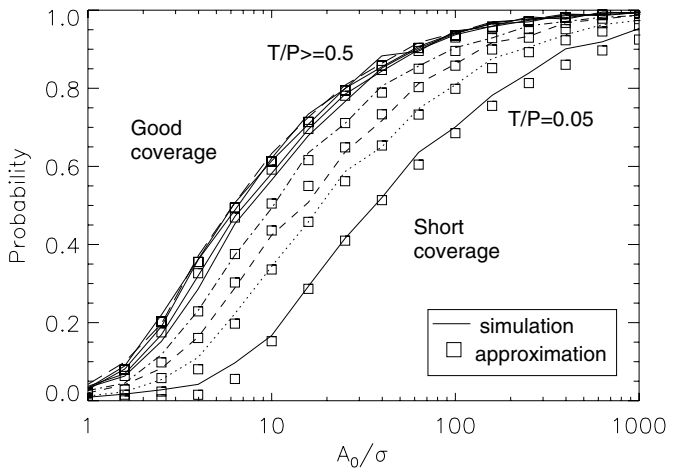

Figure 7. Probability of detecting a spectroscopic binary $p_{\rm det}$ as a function of $\kappa = A_0/\sigma_{\rm RV}$ for the case $N_{\rm obs} = 3$ and increasing period coverage $T/P = (0.05, 0.1, 0.15, 0.2, 0.3, 0.5, 0.7, 2.5, 13.5)$ (lines from right to left). The analytical model is overplotted as squares; the curves are results of simulation.

4.2. Detection of Spectroscopic Binaries

Binary companions can be detected from spectra by variable RV, appearance of double lines, or presence of unusual spectral features. The RV variability is considered here, being the most general and powerful of those methods.

The RV data are characterized by the time span T, the number of measurements $N_{\rm obs}$, and their intrinsic precision $\sigma_{\rm RV}$. The generally accepted criterion of RV variability is related to the normalized RV variance χ^2, declaring all targets with the low χ^2 probability $P(\chi^2) < 0.01$ as RV variables (Duquennoy & Mayor 1991; Nordström et al. 2004). This criterion implies the false-alarm probability of 1%, meaning that about 40 false detections are expected among the 4080 FG-67 targets surveyed by Nordström et al. Here we use the same $P(\chi^2)$ criterion, evaluate the detection probability as a function of $(N_{\rm obs}, T, \sigma_{\rm RV})$ by numerical simulation, and fit the results by a formula, as in Tokovinin (1992).

The semi-amplitude of RV variation K_1 depends on the period, mass ratio, orbital inclination i, and eccentricity e,

$$K_1 = A_0 \sin i (1-e^2)^{-1/2},$$
$$A_0 = 213 P^{-1/3} M_2 (M_1+M_2)^{-2/3}. \quad (4)$$

Here A_0 (the semi-amplitude for a circular orbit at $i = 90^\circ$, in km s^{-1}) is related to the orbital period P (in days) and the component masses M_1 and M_2 (in solar-mass units).

In the simulations, we assume normally distributed measurement errors with rms $\sigma_{\rm RV}$. For each value of three detection parameters $(N_{\rm obs}, T/P, \kappa = A_0/\sigma_{\rm RV})$, a set of 1000 artificial binaries is created. Each binary has a random eccentricity e distributed in the interval [0,1] as $f(e) = (\pi/2)\ \sin(\pi e)$, random inclination i (uniform distribution of $\cos i$), random argument of periastron, and random orbital phase. The $N_{\rm obs}$ random moments of observations are uniformly distributed; the interval T between the first and the last measurement equals the specified period fraction T/P. Obviously, for integer T/P values the first and the last observations occur at the same orbital phase; in this case SB1 cannot be detected with $N_{\rm obs} = 2$.

There are two distinct regimes of spectroscopic binary detection. When more than half of the orbit is covered ($T/P > 0.5$), the duration of observations does not matter (except the above-mentioned case $N_{\rm obs} = 2$), and the detection probability $p_{\rm det}$ is a function of only two parameters $(N_{\rm obs}, \kappa)$. On the other hand, when the observations cover only a small fraction of the period, $T/P < 0.1$, the observed RV variation is essentially a linear trend. In this regime, the first and the last observations have the most weight for the detection, which becomes almost independent of $N_{\rm obs}$. The RV variation is proportional to T, so the minimum detectable amplitude $A_0/\sigma_{\rm RV} \propto 1/T$. Indeed, the simulations show that the curves $p_{\rm det}(\kappa)$ are identical in the cases $T/P = 0.1$ and $T/P = 0.01$ if the arguments are scaled 10 times. In the intermediate situation $0.1 < T/P < 0.5$, the detection probability depends on all three parameters.

The detection probability found from the simulations can be fitted by the formula

$$p_{\rm det}(y) = \frac{y^\alpha}{y^\alpha + 2 + y^{-2.5}}, \quad y = \frac{A_0}{\sigma_{\rm RV}\kappa_0}. \quad (5)$$

The parameter κ_0 equals normalized amplitude where the detection probability is 1/4, and the parameter α regulates the steepness of the curve (steeper for larger α).

We describe the behavior of the fitting parameters (κ_0, α) by formulas that work well in both regimes and adequately represent the transition (squares in Figure 7):

$$\kappa_0 = \max[(1+0.65P/T), 2.9(N_{\rm obs}-1)^{-0.25}] \quad (6)$$

$$\alpha = \min(0.7 + T/P, \alpha_0), \quad (7)$$

where $\alpha_0 = 0.95$ for $N_{\rm obs} = 2$ and $\alpha_0 = 1.25$ for $N_{\rm obs} \geqslant 3$. In the short-coverage regime, the values of (κ_0, α) are defined by the first terms and do not depend on the number of observations. In the good-coverage case of $T/P > 0.5$, the dependence on T vanishes, the steepness of the $p_{\rm det}(\kappa)$ curves becomes constant, and the detection threshold κ_0 improves slowly with increasing number of observations $N_{\rm obs}$. The SB1 detection model (Equations (5)–(7)) is not very accurate (a few percent error), but is adequate for the statistical description. Compared to the imaging, the RV method is more "probabilistic" because $p_{\rm det} < 1$ for a wide range of parameters.

Subsystems in the secondary components of visual binaries can be detected by RV observations of the combined (blended) light if $\rho < 1\farcs5$ (e.g., HIP 518 in Figure 3), but with a reduced probability. Many visual binaries in the FG-67 sample have periods $P < 100$ yr, so that small RV variations or trends are attributable to the motion of the visual binary and/or variable component blending, rather than to a subsystem. We assume that the RV detection of a subsystem in the blended spectra is possible only when the coverage is good, $T/P > 2.5$, and the rms RV of the blended spectrum is larger than 3 km s^{-1}. Alternatively, moving lines of the binary secondary component B can be detected directly in the blended spectrum when they are strong, $\Delta m_{\rm AB} < 1.5$, and well separated from the lines of A, $A_0 > 15$ km s^{-1}.

Both criteria for detecting the spectroscopic binary in component B were included in the simulations. It turns out that the resulting detection probability can be described by Equation (5) with parameters $y = A_0(1-r)/[\kappa_0(1+r)]$, $\kappa_0 = (8 + 2\Delta m_{\rm AB})$, and $\alpha = 2.5$, provided that $N_{\rm obs} \geqslant 3$. The additional factor $(1-r)/(1+r)$, where $r = q^{3.75}$ is the light ratio in the subsystem Ba,Bb, accounts for blending of the secondary lines; when $r = 1$, the blended RV does not change at all. The existing RV data on close visual binaries are thus useful for constraining the

frequency of spectroscopic subsystems in both components, although for the secondary the detection power is much less than for the primary.

A few double-lined binaries were detected from single spectra. We assign fake detection parameters $T = 100$ days, $N = 3$, and $\sigma_{RV} = 2$ km s^{-1} to cover these cases by the same model (5), but do not apply this recipe to single stars with one RV datum. A single RV measurement of both components of a wide binary tells us that the binary is physical if the RVs match. In such a case, inner subsystems are unlikely, but this information is not included here in the detection model.

4.3. Detection of Astrometric Binaries

For the reasons outlined above, we accept only the $\Delta\mu$ binaries from Makarov & Kaplan (2005) as valid detections. It is shown by Tokovinin et al. (2012) that orbital periods of $\Delta\mu$ binaries range from a few to a hundred years.

The motion of the photo-center μ_0 (mas yr^{-1}) caused by a "dark" companion in a circular face-on orbit is related to the semi-major axis of the astrometric orbit α, which, in turn, is expressed through the orbital period P (years), primary mass M_1 (solar mass), parallax p_{HIP}, mass ratio q, and light ratio r:

$$\mu_0 = \frac{2\pi\alpha}{P} = 2\pi P^{-1/3} M_1^{1/3} p_{HIP} \frac{q-r}{(1+q)^{2/3}(1+r)}. \quad (8)$$

We assume $r = q^{3.75}$, as appropriate for dwarfs less massive than the Sun in the V band.

In the simulations of acceleration binaries, the orbit orientation, phase, and eccentricity are random (see Section 4.2). The "orbital" component of the PM is calculated by a linear fit to 10 positions of the photo-center over the time base of 3.2 yr (duration of the *Hipparcos* experiment). A similar calculation is done over the 100 yr time base of *Tycho*, and the difference gives $\Delta\mu$. To remove the dependence on parallax and q, the result is normalized by μ_0; some dependence on the binary period remains.

The cumulative distribution of $\Delta\mu/\mu_0$ is approximated analytically as

$$F(\Delta\mu/\mu_0 < \xi) \approx y^a/(y^a + y^{-b} - 1), \quad y = (\xi/\xi_0). \quad (9)$$

The cumulative probability F should be truncated at 1 (the formula gives values $F > 1$).

The parameters of the approximating formula (9) ξ_0, a, and b were fitted to the simulations for binary periods ranging from 3 yr to 500 yr. Then each parameter was approximated by a polynomial of $x = \log P$, enabling analytical calculation of F.

This statistical model allows us to evaluate the detection probability for $\Delta\mu$ binaries. For each combination of the binary period P and mass ratio q—a point in the (P, q) plane—we calculate μ_0 (the parallax is known), assume the detection threshold $\Delta\mu > 5$ mas yr^{-1} as appropriate for *Hipparcos*, and calculate $F(\Delta\mu < 5)$ using Equation (9). The detection probability is $1 - F$. It peaks around $q \approx 0.5$.

The above model does not account for binaries with short periods that can be detected by the *Hipparcos* acceleration $\dot{\mu}$, rather than by the $\Delta\mu$ method. Most such binaries are either confirmed spectroscopically (and hence have valid RV detection limits) or rejected. A few binaries with astrometric orbits and no RV data are described by a fake RV coverage in the DET table.

4.4. Detection of Wide Companions

In this subsection, we cover the detection of companions with $\rho > 3''$—a regime where confusion with background sources increases with separation.

Companion detection limits in the 2MASS Point Source Catalog are determined empirically by plotting $\Delta K_s(\rho)$ (Figure 8 in Tokovinin 2011). We adopt the "realistic" limit for $3'' < \rho < 30''$ (see Table 3). In crowded fields, companions selected from 2MASS by their colors are confused with background stars. We characterize crowding by N^*—the number of 2MASS sources within $150''$ from the target. It is assumed here that 730 targets with $N^* > 100$ are not screened for companions with 2MASS (however, the *Hipparcos* and WDS detection limits are still valid for them).

Wide binaries are also found in the WDS. The large time base of the WDS allows discrimination of optical companions by their relative motion; hence, the WDS threshold in Table 3 is applied to all targets out to $30''$ separation.

At separations $\rho > 30''$, we used the SUPERBLINK catalog and selected CPM companions by both color and PM (Tokovinin & Lépine 2012). The companion search is 90% complete to $V = 19^m$. Only 2966 targets (61% of the sample) with PM above the SUPERBLINK limit (40 mas yr^{-1} north of $-20°$ and 150 mas yr^{-1} otherwise) are covered. Most CPM companions have separations $\rho < 300''$ (projected separation less than 20,000 AU at 67 pc).

CPM pairs wider than $30''$ are also found in the WDS or by matching the *Hipparcos* stars in PM and parallax (e.g., Shaya & Olling 2011). Some of these binaries have PM below the SUPERBLINK limit or were missed by it for other reasons. We add fictitious imaging data to the DET table to cover those exceptions, with a reference "CPM."

Note that identification of wide binaries by common PM and matching colors introduces a bias against hierarchical multiples because their subsystems perturb both PM and photometry. Partially resolved secondary components will not appear in the catalogs such as SUPERBLINK. As this bias is difficult to quantify, it is silently ignored in the statistical analysis.

4.5. Average Detection Probability

The probability of companion detection is evaluated for each individual primary target. First, the resolution limits of *Hipparcos* and WDS are applied to all targets. The limits from 2MASS are added for targets with $N^* < 100$. The SUPERBLINK limit $V < 19$ and $\rho > 30''$ is applied to targets with a fast enough PM. Then the individual imaging limits are added from the DET table, when available. The resulting curve $q_{min}(P)$ splits the (P, q) plane into two parts, with $p_{det} = 1$ above it and $p_{det} = 0$ below. This sharp limit is softened to account for the fact that the detection depends on the apparent (projected) separation, which, for a given period, is random (see Section 3.9). If, at a given mass ratio, the companion becomes resolvable at some period P^*, we assign detection probability of 1/3 to periods $P^*/1.6 < P < P^*$, 2/3 to $P^* < P < 1.6P^*$, and 1 to longer periods.

The probability of resolving a companion is combined with the astrometric detection (Equation (9)) and with the RV detection (if the RV data are available) to evaluate the detection probability $p_{det} = 1 - \Pi_i(1 - p_i)$ resulting from the combination of i independent techniques. Calculation of detection limit for one target is illustrated in Figure 8.

Figure 9 shows the average $p_{det}(P, q)$ for all primary targets in the FG-67 sample. The combination of observing techniques

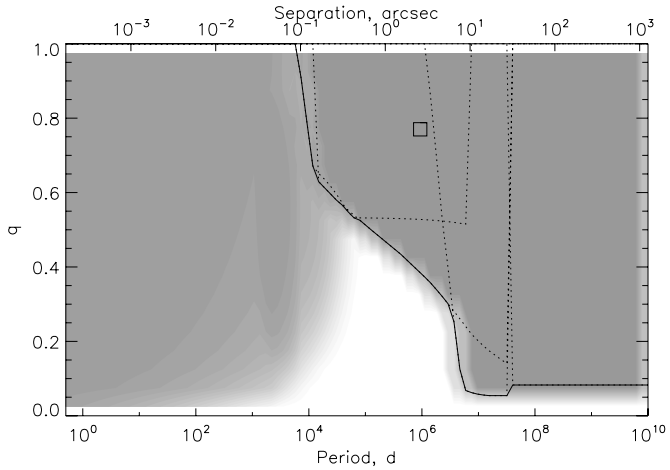

Figure 8. Probability of companion detection for HIP 55 ($p_{\rm HIP} = 15.4$ mas). Individual limits for resolved companions from *Hipparcos*, WDS, 2MASS, and CPM are plotted as dotted lines, and the combined limit as a solid line. No data from AO or speckle interferometry are available for this target. The visual companion B at 3.″8 (square) is listed in the WDS and 2MASS. The gray shading shows the combination of spatial resolution with limits resulting from *Hipparcos* acceleration $\Delta\mu$ and from the five RV measurements over time interval $T = 1394$ days by Nordström et al. (2004).

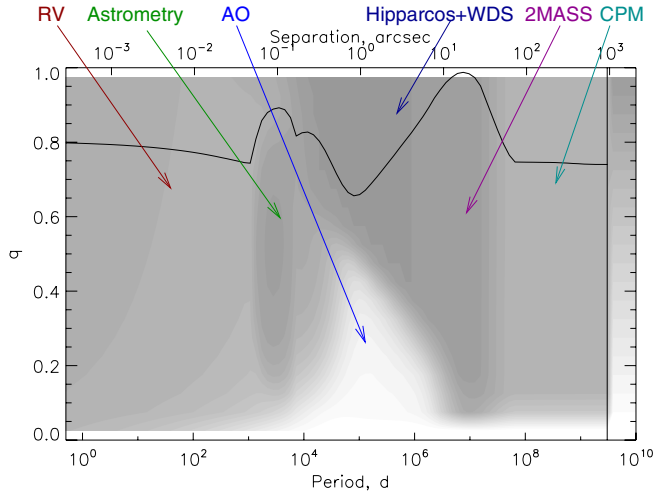

Figure 9. Average probability of companion detections around primary targets as a function of period P and mass ratio q. The color bar on the right indicates the scale, from $p_{\rm det} = 0$ (white) to $p_{\rm det} = 1$ (gray). The black curve shows detection probability averaged over $q > 0.1$. Dominant detection techniques are indicated on the top. The upper scale shows angular separation at a distance of 50 pc.

(A color version of this figure is available in the online journal.)

covers the parameter space rather uniformly, with the exception of low-mass companions with separations from 0.″3 to 10″ that are too close for the 2MASS and too faint for the WDS. Such companions can be probed with AO (which, so far, was used only on a small subset of targets).

For the *secondary* components the detection probability is evaluated separately. The *Hipparcos* detection limits in resolution and acceleration apply to the bright secondaries with individual HIP numbers and separations >20″ (at closer separations, the two stars were treated by *Hipparcos* as a binary and any subsystems were missed because resolved triple stars were not considered in the data reduction). The secondary components observed individually in RV or by imaging are also treated in the same way as the primaries. Additionally, detection data on the primary components of close visual binaries are

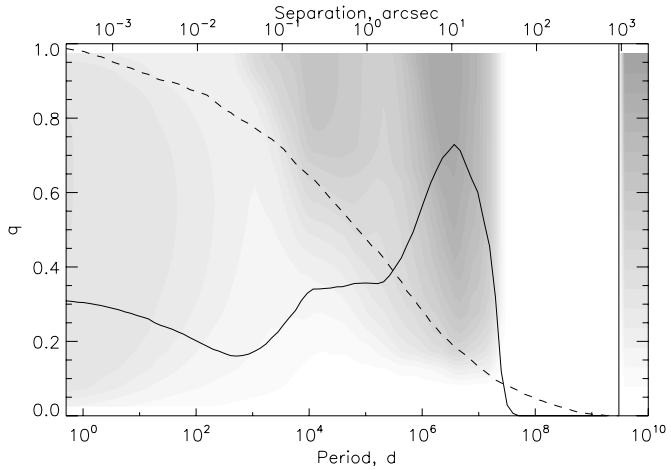

Figure 10. Average probability of detecting subsystems in the secondary components. The color scale is from 0 (white) to 1 (gray), the black curve shows detection probability averaged over q and over relevant secondaries, and the dashed line shows the fraction of relevant secondaries.

used to constrain subsystems in their secondaries, as explained in Section 4.1 and Section 4.2.

Figure 10 illustrates the average probability of detecting subsystems in the secondary components. The curve shows the probability averaged over $q > 0.05/M_2$ (i.e., ignoring any brown-dwarf companions) for the relevant secondaries (at each period of a potential subsystem, relevant secondaries are those where such subsystems are allowed dynamically by the outer binaries). The proportion of relevant secondaries is plotted as a dashed curve. Only 1676 secondaries with estimated mass (77% of their total number) are considered. There are no constraints on subsystems in the remaining 23% of secondaries belonging to the spectroscopic and astrometric binaries with unknown periods.

The estimated detection rate of subsystems in the secondary components is less than for the primaries, about 0.3 at short periods, 0.16 at periods around 1 yr, and 0.34 at periods around 30 yr. The average probability of detecting a secondary subsystem with $P \sim 10^4$ days and $q > 0.8$ is about 0.58, owing to the high-resolution imaging surveys of solar-type stars with Robo-AO (Riddle et al. 2014, in preparation) and at SOAR. At separation >3″, the subsystems are constrained by the classical imaging (e.g., 2MASS). A targeted RV survey of secondaries is obviously needed to reach better coverage at short periods. More than half of subsystems in the secondaries still remain undiscovered. Previous work on multiplicity (e.g., Raghavan et al. 2010) focused on the companions to main targets and neglected potential binarity of the secondaries (some binary secondaries within 25 pc are recovered here).

5. DESCRIPTION OF THE TABLES

5.1. COMP: Data on Individual Components

Table 4 contains identifiers, coordinates, and photometry of known components, both primary and secondary. Most resolved secondary components with separations above 1″ have individual entries in Table 4. Some bright secondaries have HIP or HD numbers. The notion of "resolved component" is fuzzy, however, so a few components are not in this table despite having $\rho > 1''$. Optical components are not included, except a few.

The columns of Table 4 contain (1) HIP0 number, (2) HIP number, which equals HIP0 for the primary target, (3) HD identifier, and (4) component designation by a capital letter,

Table 4
COMP: Data on Individual Components

HIP0	HIP	HD	Comp.	ρ	θ	R.A., decl. (J2000)		$\mu_{\alpha*}$	μ_δ	$p_{\rm HIP}$	···	V	I_C	J	K_s	N^*
				($''$)	(deg)	(deg)	(deg)	(mas yr^{-1})		(mas)	···	(mag)	(mag)	(mag)	(mag)	
(1)	(2)	(3)	(4)	(5)	(6)	(7)	(8)	(9)	(10)	(11)	···	(15)	(16)	(17)	(18)	(19)
50	50	224782	A	0.0	0.0	0.143085	−53.097713	52.9	−20.9	16.8	···	6.49	5.81	5.41	5.05	14
50	0	0	B	1.6	331.0	0.142726	−53.097325	0.0	0.0	16.8	···	9.85	0.00	0.00	0.00	14
55	55	224783	A	0.0	0.0	0.158834	−66.683174	162.8	−28.9	15.4	···	7.40	6.78	6.53	6.21	18
55	0	0	B	3.8	274.0	0.156173	−66.683100	0.0	0.0	15.4	···	9.17	0.00	6.80	6.40	18
58	58	224792	A	0.0	0.0	0.173513	62.175899	−46.9	−43.8	25.8	···	7.05	6.46	6.07	5.81	208
81	81	224828	A	0.0	0.0	0.243409	−4.932534	−184.6	−172.6	22.8	···	8.57	7.86	7.34	6.96	10

(This table is available in its entirety in machine-readable and Virtual Observatory (VO) forms in the online journal. A portion is shown here for guidance regarding its form and content.)

Table 5
SYS: Data on Binary Systems

HIP0	Comp.	Type	ρ		θ	V_1	V_2	P		M_1		M_2		Comment
(1)	(2)	(3)	(4–5)		(6)	(7)	(8)	(9–10)		(11–12)		(13–14)		(15)
50	A,B,*	Ch	1.49	”	331.0	6.55	9.85	534.99	y	1.55	v	0.87	v	HJ_5437
55	A,B,*	Chp	3.800	”	274.0	7.69	9.17	2.556	k	1.31	v	1.00	v	GLI_289
93	Aa,Ab,*	s,a,v	0.330	”	73.0	8.12	15.98	76.17	y	1.18	v	0.24	k	CfA:P=long MK05:dmu NICI
179	Aa,Ab,*	S2	2.008	m	0.0	6.91	0.00	10.674	d	1.32	v	1.32	q	N04:drv=30.5* Orb.Gorynya2013
223	A,B,*	v	1.600	”	163.0	7.40	9.36	397.08	y	1.17	v	0.84	v	BU_281AB
223	X A,C	Xph	44.300	”	330.0	7.40	11.70	0.000	y	0.00	···	0.00	···	HJ_998AC Reflex PM
290	Aa,Ab,*	s,a	0.000	”	0.0	7.78	0.00	0.000	y	1.29	v	0.00	···	N04:drv=1.3 MK05:dmu
305	X Aa,Ab	a?	0.000	”	0.0	7.81	0.00	0.000	y	1.13	v	0.00	···	HIP:7 N04:RV=const WSI:UR

(This table is available in its entirety in machine-readable and Virtual Observatory (VO) forms in the online journal. A portion is shown here for guidance regarding its form and content.)

Table 6
DET1: Detection Limits in Radial Velocity

HIP0	Comp	T (days)	$N_{\rm obs}$	$\sigma_{\rm RV}$ (km s^{-1})	Ref.
50	AB	683	3	0.300	N04
50	B	208	3	0.020	Nid02
55	AB	1394	5	0.400	N04
58	A	1168	2	0.300	N04
58	A	4109	9	0.300	CfA
81	A	4433	13	0.610	Latham2002

(This table is available in its entirety in machine-readable and Virtual Observatory (VO) forms in the online journal. A portion is shown here for guidance regarding its form and content.)

generally matching the WDS designations. Then follow (5) separation from the primary in arcseconds and (6) position angle of the companion. Both these fields are zero for primary targets. Columns (7) and (8) contain equatorial coordinates for J2000 in the ICRS system, taken from HIP2 in most cases. If only the relative position of the secondary component is known from the WDS, its coordinates are calculated with reference to the primary. Coordinates of some secondary components are taken from 2MASS.

Columns (9), (10), and (11) list the PM $\mu_{\alpha*}$, μ_δ, and the parallax $p_{\rm HIP}$ taken from HIP2 for the main targets and for the secondaries with separate HIP entries. For other secondary components, the parallax equals that of the main target by definition; the PM is zero, if not measured independently. Sources of PM for the secondary components are WDS, PPMX (Roeser et al. 2008), NOMAD (Zacharias et al. 2004), or SUPERBLINK. Errors of the PM and parallax are listed in columns (12)–(14) when available, zero otherwise (these columns are omitted from the printed fragment of the table to save space).

Magnitudes in the V, I_C, J, and K_s bands are given in columns (15)–(18), respectively, taken mostly from HIP2 and 2MASS. Other sources (e.g., WDS and NOMAD) are invoked to complement the photometry of secondary components, whenever possible. Photometric information helps to identify physical companions by their position on the CMDs. The last column (19) of Table 4 lists N^*, the number of point sources in the 2MASS catalog within 150$''$ of each primary target, to quantify the density of the stellar background.

5.2. SYS: Data on Binary Systems

A hierarchical multiple system consists of several binaries, where some components are actually pairs of stars. Each binary system or subsystem corresponds to a line in Table 5. It contains the *Hipparcos* number of the primary target HIP0 in column (1) and the designation of the system by a comma-separated list of its components (primary, secondary, parent) in column (2). Then in column (3) the type of the system is listed by codes explained above in Section 3. Optical pairs from the WDS and other spurious binaries are kept in the SYS table for completeness and are distinguished by their component designation starting with “X.”

Columns (4), (5), and (6) list the separation and its units (“ for arcseconds, m for milliarcseconds) and the position angle in degrees (zero if unknown). Visual magnitudes of the components are given in columns (7) and (8). The orbital period and its units (“d,” “y,” “k” for days, years, and kiloyears, respectively) are in columns (9) and (10). The estimated masses of the primary and secondary components with one-letter codes

Table 7
DET2: Imaging Detection Limits

HIP0 (1)	Comp (2)	λ (3)	ρ_1 (4)	ρ_2 (5)	ρ_3 (6)	ρ_4 (7)	Δm_1 (8)	Δm_2 (9)	Δm_3 (10)	Δm_4 (11)	Ref. (12)
50	A	540.0	0.029	0.150	1.000	1.500	0.50	5.51	6.50	6.50	SOAR
81	A	550.0	0.030	0.100	0.200	1.500	0.00	1.35	2.70	3.00	WSI
93	A	2272.0	0.054	0.150	0.900	9.000	0.00	5.26	7.15	7.15	NICI
135	A	550.0	0.030	0.100	0.200	1.500	0.00	1.35	2.70	3.00	WSI
179	A	550.0	0.066	0.220	0.439	1.500	0.00	0.35	2.70	3.00	INT4
179	A	770.0	0.150	0.800	2.100	13.920	2.65	5.19	6.29	6.29	RoboAO

(This table is available in its entirety in machine-readable and Virtual Observatory (VO) forms in the online journal. A portion is shown here for guidance regarding its form and content.)

Table 8
Notes

HIP0	Text
93	CfA: P=long N04:drv=1.2. SIMBAD: 14 ref.
93	Tok2012bis: Resolved with NICI at 0.″32. 72d, dK=4.3 dH=4.3. V(AB) is estimated
179	Speckle: 2001AJ....121.3224M SIMBAD: 12 ref. N04:q=1.00+-0.011 N=5 drv=30.5
179	SB2 orbit by Gorynya2013: P=10.674d, e=0.34, K1=55.00 K2=56.62, twin.
276	Cfa: SB, P=538d?

(This table is available in its entirety in machine-readable and Virtual Observatory (VO) forms in the online journal. A portion is shown here for guidance regarding its form and content.)

indicating the method (see Section 3.9) are listed in columns (11), (12) and (13), (14), respectively. The last column (15) of Table 5 contains a short comment pointing to the source of the information (e.g., WDS discoverer codes for resolved binaries, SB9 references for SBs). Bibliographic codes from Table 1 are used extensively in the comments.

5.3. DET: Individual Detection Limits

Methods used to estimate the detection limits are covered in Section 4. The data on individual components are presented in two tables, DET1 and DET2. Table 6 (7109 lines) lists the RV data, linked to the particular component by the HIP0 number in column (1) and the component identifier in column (2). Then the time coverage T in days, the number of observations $N_{\rm obs}$, and the measurement precision $\sigma_{\rm RV}$ in km s^{-1} are given in columns (3)–(5), respectively, followed by the bibliographic reference in column (6). The reference codes match the references in Table 1.

The detection limits of imaging (AO and speckle) are listed in Table 7 (DET2, 4165 lines). Columns (1) and (2) contain the HIP0 and component, as in Table 6. Then in column (3) the imaging wavelength in nm is given. Columns (4)–(7) list the separations ρ_i in arcseconds, columns (8)–(11) contain the corresponding detection limits Δm_i, and column (12) gives the reference code.

5.4. Notes

Notes are given in Table 8 as free text linked to the HIP0 number of the target. The references are denoted by the codes from Table 1 or given explicitly in the notes.

6. OVERVIEW

The SYS table contains 3068 pairs, 2196 of which are physical; the rest are optical or spurious. Periods of 357 binaries remain unknown (208 of "a" type and 261 of "s" type, with an overlap of 112 between those groups). It is safe to assume that all unknown periods are shorter than 100 yr. The proportion of unknown periods among 1132 systems with $P < 100$ yr is 32%.

This rich material is used in the accompanying Paper II to study the statistics of hierarchical stellar systems. The data collected here can be useful for several other purposes, for example, to complement exoplanet programs, to search for Sirius-like binaries, to select fast resolved pairs for orbit calculation, or to study relative motion in wide binaries and resolved triples. The weakness of this sample—missing information on many spectroscopic and astrometric binaries—can be corrected in the future by RV monitoring and high-resolution imaging.

I am grateful to D. Latham (CfA) and B. Mason (USNO) for sharing their unpublished data. This project benefited from fruitful collaboration with M. Hartung, S. Lépine, R. Riddle, N. Gorynya, and others.

This work used the SIMBAD service operated by Centre des Données Stellaires (Strasbourg, France), bibliographic references from the Astrophysics Data System maintained by SAO/NASA, data products of the Two Micron All-Sky Survey (2MASS), the Washington Double Star Catalog maintained at USNO, and the SB9 catalog managed by D. Pourbaix. It is a suitable occasion to celebrate the often neglected effort of those who maintain catalogs and databases and thus keep the foundation of astronomy solid.

Facilities: SOAR, CTIO: 1.3m

REFERENCES

Abt, H. A., & Willmarth, D. 2006, ApJS, 162, 207
Anderson, E., & Francis, C. 2012, AstL, 38, 331
Baraffe, I., Chabrier, G., Allard, F., & Hauschildt, P. H. 1998, A&A, 337, 403
Caballero, J. A. 2010, A&A, 514, 98
Casagrande, L., Schönrich, R., Asplund, M., et al. 2013, A&A, 530, 138
Chauvin, G., Lagrange, A.-M., Bonavita, M., et al. 2010, A&A, 509, 52
Chauvin, G., Lagrange, A.-M., Udry, S., et al. 2006, A&A, 456, 1165
Cutri, R. M., Skrutskie, M. F., van Dyk, S., et al. 2003, The IRSA 2MASS All-Sky Point Source Catalog. NASA/IPAC Infrared Science Archive
Delfosse, X., Forveille, T., Ségransan, D., et al. 2000, A&A, 364, 217
Duquennoy, A., & Mayor, M. 1991, A&A, 248, 485

Eggenberger, A., Udry, S., Chauvin, G., et al. 2007, A&A, 474, 273
Fabrycky, D., & Tremaine, S. 2007, ApJ, 669, 1298
Frankowski, A., Jancart, S., & Jorissen, A. 2007, A&A, 464, 377
Ginski, C., Mugrauer, M., Seeliger, M., & Eisenbeiss, T. 2012, MNRAS, 421, 2498
Girardi, L., Bressan, A., Bertelli, G., & Chiosi, C. 2000, A&A, 141, 371
Goldin, A., & Makarov, V. V. 2006, ApJS, 166, 341
Griffin, R. F. 2012, JApA, 33, 29
Halbwachs, J.-L., Mayor, M., & Udry, S. 2012, MNRAS, 422, 14
Hartkopf, W. I., & Mason, B. D. 2013, Sixth Catalog of Orbits of Visual Binary Stars, USNO, http://ad.usno.navy.mil/wds/orb6.html
Hartkopf, W. I., Mason, B. D., Finch, C. T., et al. 2013, AJ, 146, 76
Hartkopf, W. I., Mason, B. D., & McAlister, H. A. 2001, AJ, 122, 3480
Henry, T. J., & McCarthy, D. W. 1993, AJ, 106, 773
Holberg, J. B., Oswalt, T. D., & Sion, E. M. 2013, MNRAS, 435, 2077
Horch, E. P., Gomez, S. C., Sherry, W. H., et al. 2011, AJ, 141, 45
Janson, M., Brandt, T. D., Moro-Martín, A., et al. 2013, ApJ, 773, 73
Jenkins, J. S., Jones, H. R. A., Biller, B., et al. 2010, A&A, 515, 17
Jódar, E., Pérez-Garrillo, A., Díaz-Sánchez, A., et al. 2013, MNRAS, 429, 859
Jones, H. R. A., Butler, P. R., Marcy, G. W., et al. 2002, MNRAS, 337, 1170
Lafrenière, D., Doyon, R., Marois, Ch., et al. 2007, ApJ, 670, 1367
Lagrange, A.-M., Desort, M., Galland, F., et al. 2009, A&A, 495, 335
Lang, K. R. 1992, Astrophysical Data I. Planets and Stars (Berlin: Springer)
Latham, D. W., Stefanik, R. P., Torres, G., & Davis, R. J. 2002, AJ, 124, 1144
Makarov, V. V., & Kaplan, G. H. 2005, AJ, 129, 2420
Mason, B. D., Wycoff, G. L., Hartkopf, W. I., Douglass, G. G., & Worley, C. E. 2001, AJ, 122, 3466
Metchev, S. A., & Hillenbrand, L. A. 2009, ApJS, 181, 62
Nidever, D. L., Marcy, G. W., Butler, R. P., et al. 2002, ApJS, 141, 503
Nordström, B., Mayor, M., Andersen, J., et al. 2004, A&A, 418, 989
Perets, H. B., & Fabrycky, D. C. 2009, ApJ, 697, 1048
Perryman, M. A. C., & ESA, 1997, The Hipparcos and Tycho Catalogues (ESA SP Series, Vol. 1200; Noordwijk: ESA)
Pourbaix, D., Tokovinin, A. A., Batten, A. H., et al. 2004, A&A, 424, 727
Raghavan, D., McAlister, H. A., Henry, T. J., et al. 2010, ApJS, 190, 1
Rameau, J., Chauvin, G., & Lagrange, A.-M. 2013, A&A, 553, 60
Roell, T., Neuhäuser, R., Seifahrt, A., et al. 2012, A&A, 542, A92
Roeser, S., Schilbach, E., Schwan, H., et al. 2008, A&A, 488, 401
Santerne, A., Fressin, F., Díaz, R. F., et al. 2013, A&A, 557, 139
Shaya, E. J., & Olling, R. P. 2011, ApJS, 192, 2
Soubiran, C., Le Campion, J.-F., Cayrel de Strobel, G., & Caillo, A. 2010, A&A, 515, 111
Tokovinin, A. 1997, A&AS, 124, 75
Tokovinin, A. 2011, AJ, 141, 52
Tokovinin, A., Hartung, M., & Hayward, Th. L. 2010a, AJ, 140, 510
Tokovinin, A., Hartung, M., & Hayward, Th. L. 2013, AJ, 146, 8
Tokovinin, A., Hartung, M., Hayward, Th. L., & Makarov, V. V. 2012, AJ, 144, 7
Tokovinin, A., & Lépine, S. 2012, AJ, 144, 102
Tokovinin, A., Mason, B. D., & Hartkopf, W. I. 2010b, AJ, 139, 743
Tokovinin, A., Thomas, S., Sterzik, M., & Udry, S. 2006, A&A, 450, 681
Tokovinin, A. A. 1992, A&A, 256, 121
Tokovinin, A. A., & Smekhov, M. G. 2002, A&A, 382, 118
Tremko, J., Bakos, G. A., Ziznivsky, J., et al. 2010, CoSka, 40, 83
van Leeuwen, F. 2007, A&A, 474, 653
Zacharias, N., Monet, D. G., Levine, S. E., et al. 2004, A&AS, 204, 4815